Model Predictive Control for the Wound Rotor Synchronous Machine using Piecewise Affine Flux Maps

Bernard Steyaert
Columbia University
bernard.steyaert@columbia.edu

Michael Eull
Power Networks Demonstration Centre
michael.eull@strath.ac.uk

Ethan Swint
Tau Motors
ethan@taumotors.com

W. Wesley Pennington
Tau Motors
wesley@taumotors.com

Matthias Preindl
Columbia University
matthias.preindl@columbia.edu

***Abstract*—High-performance control of Wound Rotor Synchronous Machines (WRSM) motor drives requires a nonlinear magnetic model that captures magnetic saturation and cross saturation. This includes Model Predictive Control (MPC), which has proven to be effective with similar synchronous machines such as the Permanent Magnet Synchronous Machine (PMSM). Varying the inductance depending on machine operating point is modelled using Piecewise Affine (PWA) Functions in the form of Look up Tables (LUTs). PWA functions are used to create virtual-flux in the r, d, and q-axis of the WRSM but can be extended to account for other effects such as damper windings, and zero-sequence current. A closed-loop virtual-flux Constrained Finite Time Optimal Control (CFTOC) MPC controller is formulated using PWA in the state space equations, and a simulated setup demonstrates the feasibility of the concept.**

***Index Terms*—Flux estimation, Model Predictive Control, Motor Parameters, Piecewise Linear Techniques, Torque Control, Wound Rotor Synchronous Machine (WRSM)**

I. Introduction

Electric machines produce torque by combining armature current and magnetic flux linkage. This research focuses on the wound rotor synchronous machine (WRSM) that produces the main magnetic field with a rotor winding. WRSMs are a class of electric machines used in power generation, traction (e.g., electric vehicles, EVs), and other industrial and residential applications. They have several advantages over PMSMs including: higher level of controllability due to their ability to modulate rotor flux, a large constant-power speed range, and increased cost-effectiveness given that no expensive, rare-earth magnets are required in production. However, WRSMs have certain drawbacks when compared to PMSMs including: higher copper losses due to the added rotor windings, and increase mechanical complexity. Brushes and slip rings limit power flow to the rotor, although there are designs for wireless power transfer [1]. Finally, WRSM have a strong (nonlinear) coupling between the direct (d) and rotor (r) dimension.

Electric machines use ferromagnetic materials to maximize and channel magnetic flux. Such machines tend to operate non-linear magnetic regime in general and exhibit saturation and cross saturation [1]–[9]. The relationship between current and flux linkage is modeled using Magnetic Models (MM) that are also also referred to as flux linkage maps in literature. Such maps tend to be linearized and expressed as inductances or transfer functions for motor control. All controllers use an explicit or implicit MM [10], [11].

Offline MM use one or a combination of Finite Element Analysis (FEA) [4], [7], [12], analytical calculations [3], [4], and experimental values [2]–[4], [7], [9]–[12] to measure inductances at various operating points. The discrete values obtained by these methods are linked together using a variety of methods, summarized in Table I. The majority of WRSM controllers use a linearized, offline MM. These include in sliding mode control [13], maximum torque [14], passivity-based control [15], and predictive direct current control [16]. Capturing non-linear flux is much simpler using online estimation methods. Some examples include Kalman filters [6], Flux-linkage observers [8], and iterative numerical solvers [17]. Of these only [8] uses an advanced state-space controller (DB-DTFC). Estimation and advanced control require additional microcontroller resources and/or computation time to complete closed loop control cycles.

This research proposes using PWA functions to build an offline MM LUT to capture non-linear flux. These simplify the state-space equations to be linear, decreasing computation time. The saved computation time can instead be spent solving a CFTOC MPC problem, which has not been shown in literature for a WRSM.

This paper is organized as follows. In Section II the WRSM state-space model using PWA is presented. Section III introduces the MPC optimization problem for a

TABLE I: Summary of Offline MM Linking Methods

Type of Link	**Linear**	**Bidirectional**	**Continuous**	**Differentiable**	**Saturation**	**Cross-sat.**
Linearized Inductance	•	•	•	•		
Linearly Interpolated LUT			•		•	•
Hermite and Spline LUT [12], [10], [11]			•	•	•	•
Polynomial Functions [7], [9]			•	•	•	•
Piece-wise Nonlinear Functions [2]			•	•	•	•
Other Nonlinear Functions [3], [4]			•	•	•	•
Piece-wise Linear (PWA)	•	•	•		•	•

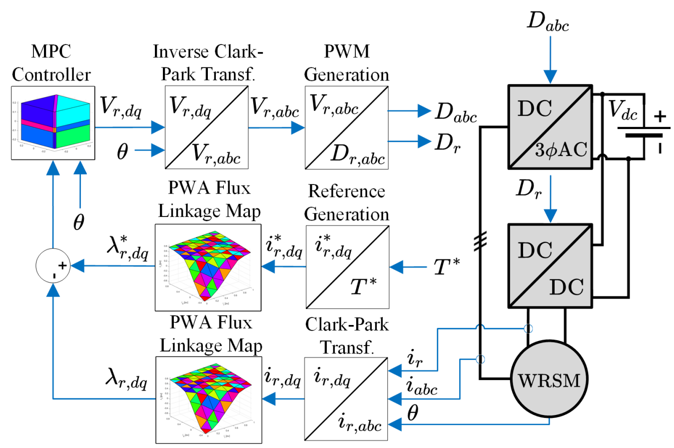

Fig. 1: WRSM motor drive (gray) with an example motor controller (white) using MPLPT function (blue) to generate reference torque from reference current

WRSM. Section IV presents results of MPC in a simulation, and Section V concludes the paper.

II. Piecewise Affine Motor Model

A. Dynamic Model and Flux Map

The three-phase WRSM can be described dynamically as a state-space model [18]. For formal simplicity and the common challenges of displaying spaces higher than three, this research focuses on the most common WRSM used in motor drives: a neutral-point isolated machine (without zero-axis flux and current) and without damper windings. However, it is noted that it is trivial to generalize this research to higher dimensions. Throughout this research, we use the power-invariant Clarke transformation and the magnetic axis of the field winding is used as reference angle of the Park transformation.

The voltage equations of this WRSM are

$$\dot{\lambda}_r = v_r - R_r i_r \qquad = \bar{v}_r, \tag{1a}$$
$$\dot{\lambda}_d = \omega\lambda_q + v_d - R_s i_d \qquad = \omega\lambda_q + \bar{v}_d, \tag{1b}$$
$$\dot{\lambda}_q = -\omega\lambda_d + v_q - R_s i_q \qquad = -\omega\lambda_d + \bar{v}_q, \tag{1c}$$

where $\dot{}$ is the $\frac{d}{dt}$ operator; $\lambda_r \in \mathbb{R}$ is the rotor, i.e. field, flux linkage; $\lambda_d, \lambda_q \in \mathbb{R}$ are the d-axis and q-axis stator flux linkages respectively; $i \in \mathbb{R}$ and $v \in \mathbb{R}$ are the currents and voltages of the appropriate dimension; $R_r, R_s \in \mathbb{R}^+$ are the rotor and stator resistances, and $\omega \in \mathbb{R}$ is the synchronous speed, i.e. the electrical velocity of the machine. Furthermore, we introduce the voltages $\bar{v}$ that are the terminal voltages compensated by the winding resistive voltage drop. This concept can be generalized to include compensation for inverter nonlinear behavior such as switch on-voltage drops and dead-times [19]. The machine currents map onto machine flux with a nonlinear map $\phi : \mathbb{R}^3 \to \mathbb{R}^3$

$$\lambda_r = \phi_r(i_r, i_d, i_q), \tag{2a}$$
$$\lambda_d = \phi_d(i_r, i_d, i_q), \tag{2b}$$
$$\lambda_q = \phi_q(i_r, i_d, i_q), \tag{2c}$$

that captures magnetic coupling between axis, magnetic saturation, and cross-saturation [18]. These equations can be written as a standard state-space systems in discrete time with sampling period T_s

$$\lambda^+_{rdq} = f(\lambda_{rdq}, \bar{v}_{rdq}), \tag{3a}$$
$$i_{rdq} = g(\lambda_{rdq}), \tag{3b}$$

where the state is the flux $\lambda_{rdq} = [\lambda_r, \lambda_d, \lambda_q]^T \in \Lambda$, the input is the compensated voltage $\bar{v}_{rdq} = [\bar{v}_r, \bar{v}_d, \bar{v}_q]^T \in \mathcal{V}$, and the measurement is the current $i_{rdq} = [i_r, i_d, i_q]^T \in \mathcal{I}$. The state-space variables are finite in all dimension that are approximated with box constraints

$$\mathcal{I} = \{i_{rdq} \in \mathbb{R}^3 | I_{\min} \leq i_{rdq} \leq I_{\max}\}, \tag{4a}$$
$$\mathcal{V} = \{\bar{v}_{rdq} \in \mathbb{R}^3 | \bar{V}_{\min} \leq \bar{v}_{rdq} \leq \bar{V}_{\max}\}. \tag{4b}$$

The flux constraint is defined as a derivative of the current constraint $\Lambda = \phi \circ \mathcal{I}$. Furthermore, the flux (and current) constraints are chosen such that the rotor flux (and current) is positive $\lambda_r \geq 0$ (and $i_r \geq 0$) without loss of generality.

The dynamic equation is expressed in vector notation as [20]

$$f_{rdq}(\lambda_{rdq}, \bar{v}_{rdq}) = (\mathbf{I} - \omega T_s \mathbf{J})\lambda_{rdq} + T_s \bar{v}_{rdq}, \tag{5}$$

where $\mathbf{J}$ is the 90° rotation matrix in the dq plane

$$\mathbf{J} = \begin{bmatrix} 0 & 0 & 0 \\ 0 & 0 & -1 \\ 0 & 1 & 0 \end{bmatrix}. \tag{6}$$

The output function $g_{rdq} : \mathbb{R}^3 \to \mathbb{R}^3$ is the inverse of the nonlinear flux map $\phi(\cdot) = [\phi_r(\cdot), \phi_d(\cdot), \phi_q(\cdot)]^T$. Typically, $\phi(\cdot)$ is bijective and the output function is defined as

$$g_{rdq}(\lambda_{rdq}) = \phi^{-1}(\lambda_{rdq}) \tag{7}$$

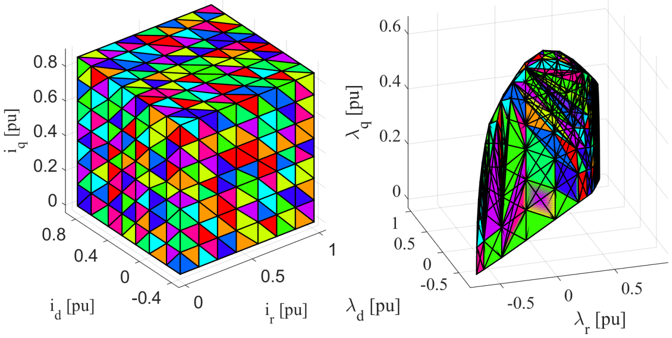

Fig. 2: Mesh of simplices $\mathcal{I}_M = \{\mathcal{I}_1, \mathcal{I}_2 \dots \mathcal{I}_m\}$ in current space (left), and mesh of simplices $\Lambda_M = \{\Lambda_1, \Lambda_2 \dots \Lambda_m\}$ (right) in flux space

The map $\phi(\cdot)$ is typically obtained with with finite element analysis (FEA) or obtained with experimental measurement campaigns. This approach describes the map $\phi(\cdot)$ by N tuples of currents i_j and flux linkage λ_j with $j \in \{0, 1, \dots, N\}$. The sets of points containing all measurements $\mathcal{I}_P = \{i_1, \dots, i_N\} \subset \mathcal{I}$ and $\Lambda_P = \{\lambda_1, \dots, \lambda_N\} \subset \Lambda$ are assumed to be in a general position to define a lookup table (LUT) that approximates the map $\phi(\cdot)$. The data is typically ordered in the first variable to simplify searching a LUT.

The equation for relating current to flux linkage in the WRSM without saturation has the form

$$\lambda_{rdq} = \mathbf{L}_{rdq} i + \psi_{rdq}, \tag{8}$$

where $\mathbf{L}_{rdq} \in \mathbb{R}^+_{3\times3}$ is the inductance matrix and $\psi_{rdq} \in \mathbb{R}_{3\times1}$ is the flux-offset vector

$$\mathbf{L}_{rdq} = \begin{bmatrix} L_{rr} & L_{rd} & L_{rq} \\ L_{dr} & L_{dd} & L_{dq} \\ L_{qr} & L_{qd} & L_{qq} \end{bmatrix}, \quad \psi_{rdq} = \begin{bmatrix} \psi_r \\ \psi_d \\ \psi_q \end{bmatrix}. \tag{9}$$

The diagonal terms of $\mathbf{L}$ are the self-inductances of the rotor (L_{rr}) and stator (L_{dd}, L_{qq}), while the non-diagonal terms are the mutual inductances between the three axis. Typically L_{rq}, L_{dq}, L_{qr}, and L_{qd} are negligible while L_{dr} and L_{rd} create the cross coupling effect.

B. Alpha-Beta Form

If the $\alpha\beta$ form is preferred, the measured currents and fluxes become

$$\lambda_{r\alpha\beta} = \mathbf{P}^{-1}(\lambda_{rdq}) \tag{10a}$$
$$i_{r\alpha\beta} = \mathbf{P}^{-1}(i_{rdq}) \tag{10b}$$
$$\tag{10c}$$

where $\mathbf{P}^{-1}$ is the inverse Park transform matrix. The dynamic equation can be re-derived in matrix form as

$$f_{r\alpha\beta}(\bar{v}_{r\alpha\beta}) = T_s \bar{v}_{r\alpha\beta}, \tag{11}$$

with the cross coupling speed ω terms eliminated. The output function becomes

$$g_{r\alpha\beta} = \mathbf{P}^{-1}(\theta)\, \phi^{-1}(\mathbf{P}(\theta)\, \lambda_{r\alpha\beta}). \tag{12}$$

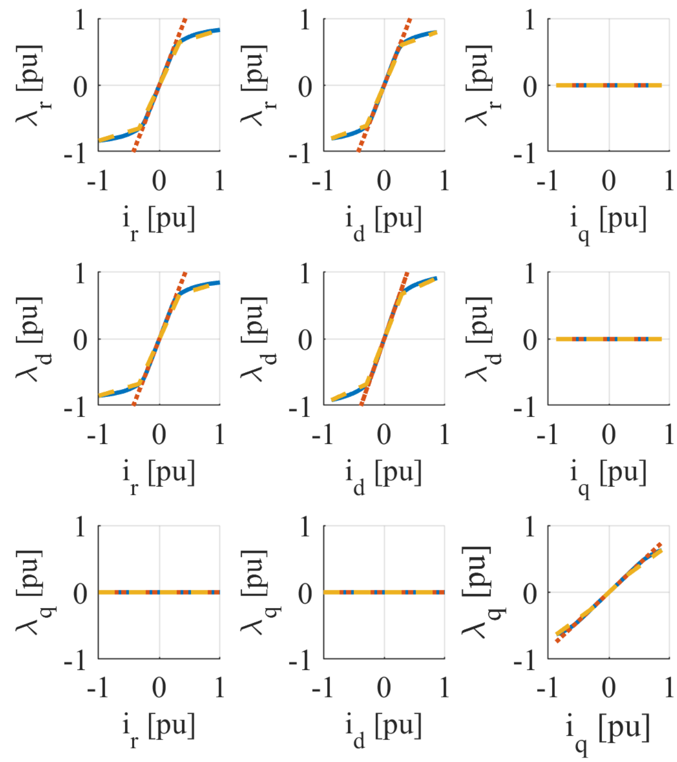

Fig. 3: WRSM flux vs current: experimental (blue), example linearization through origin (orange), example of three-segment PWA (yellow)

C. PWA Domains and Flux Maps

This research proposes to express the WRSM magnetic model as piecewise-affine (PWA) map. PWA maps divide a nonlinear map into M domains over which the function is linearized [21]. Hence we express the PWA current to flux map as

$$\lambda = \phi(i) \approx \phi_{PWA}(i) = \begin{cases} \mathbf{L}_1 i + \psi_1, & i \in \mathcal{I}_1, \\ \mathbf{L}_2 i + \psi_2, & i \in \mathcal{I}_2, \\ \quad \dots & \\ \mathbf{L}_M i + \psi_M, & i \in \mathcal{I}_M, \end{cases} \tag{13}$$

where $\lambda = \mathbf{L}_j i + \psi_j$ is the affine equation that maps currents $i \in \mathcal{I}_j$ onto fluxes $\lambda \in \Lambda_j$ and Λ_j is the image of the domain $\mathcal{I}_j$. An example PWA is shown in Figure 3.

Similarly, we can express the PWA flux to current map

$$i = \phi^{-1}(\lambda) \approx \phi^{-1}_{PWA}(\lambda) = \begin{cases} \mathbf{L}_1^{-1}\lambda + \mathbf{L}_1^{-1}\psi_1, & \lambda \in \Lambda_1, \\ \mathbf{L}_2^{-1}\lambda + \mathbf{L}_2^{-1}\psi_2, & \lambda \in \Lambda_2, \\ \mathbf{L}_M^{-1}\lambda + \mathbf{L}_M^{-1}\psi_M, & \lambda \in \Lambda_M. \end{cases} \tag{14}$$

The affine map is defined by the the inductance matrix and a flux offset. Figure 4 shows $\phi_{PWA}(i)$ in various resolutions.

PWA maps divide the original domain into M sets. We define each subset to be a simplex, which is the simplest possible polytope in any D-dimensional space and a tetrahetron in the three dimensions of the given problem. A D-dimensional simplex can be defined as the convex hull of its $D+1$ vertices (called the V-notation; alternatively, a simplex can be defined by its by its faces defined as affine inequalities called the H-notation [22])

$$\mathcal{I}_j = \mathcal{H}(\{i_{j_0}, i_{j_1}, \ldots, i_{j_D}\}), \tag{15}$$

where $i_{j_0}, \ldots, i_{j_D} \in \mathcal{I}_P$. Each current simplex $\mathcal{I}_j$ forms a domain of an affine map that maps into the flux simplex

$$\Lambda_j = \mathcal{H}(\{\lambda_{j_0}, \lambda_{j_1}, \ldots, \lambda_{j_D}\}), \tag{16}$$

where $\lambda_{j_0}, \ldots, \lambda_{j_D} \in \Lambda_P$. The general position of the defining set of measurement points implies that the vertices of each simplex are linearly independent and full dimension (not degenerate). A full current domain can thus be divided into many simplices that only overlap on their edges and adjacent faces. This simplical complex, or current mesh, $\mathcal{I}_M$ has a corresponding flux mesh Λ_M, shown in Figure 2.

III. Model Predictive Control

A. State Space Model

Model Predictive Control (MPC), or Receding Horizon Control (RHC), is a method of control that solves a constrained finite time optimal control (CFTOC) problem that finds the minimal-cost path from a start state to and end state.

In this problem the $\alpha\beta$ form of the machine equations is preferred. The state equation is equation 11 and the output equation is equation 12 both in discrete time. In the $\alpha\beta$ form, the state equation has no dependence on speed ω and is linear. For the rest of this section it can be assumed fluxes λ, currents i, and terminal voltages $\bar{v}$ are in $r\alpha\beta$ form.

B. Receding Horizon Control

RHC provides an optimal input $\bar{v}$ to the plant by computing a set of inputs $\mathcal{V}_{0\to N}$ that reaches a desired state λ_N from a starting state λ_0 in N time steps, then choosing the first value of the set. N is called the horizon length.

The known state variable at the present time k is denoted $\lambda(k)$, a calculated future state variable at time k is denoted λ_k, and the state predicted for time $t+k$ computed at time k is denoted $\lambda_{t+k|k}$. The same notation is valid for inputs $\bar{v}$.

An input trajectory of length N where the input starts at $\bar{v}_0$ is denoted as the set

$$\mathcal{V}_{0\to N} = \{\bar{v}_0, \ldots, \bar{v}_{N-1}\}. \tag{17}$$

The starting state is denoted λ_0 and the value of the input and state at the end of the trajectory are denoted $\bar{v}_N$, λ_N respectively.

A cost J_0 for a given a trajectory can be calculated by

$$J_0(\lambda_0, i_0) \triangleq \lambda_N' \mathbf{P} \lambda_N + \sum_{k=0}^{N-1} \bar{v}' \mathbf{Q} \bar{v} \tag{18}$$

where λ_k and $\bar{v}_k$ are the state and input at some time k in the trajectory.

The cost function has two components. The first is called the "terminal cost" and uses the matrix $\mathbf{P} \in \mathbb{R}^+_{3x3}$ to penalize the trajectory based on how close the final state λ_N is against the desired state. The second component is called "stage cost" which uses the matrix $\mathbf{Q} \in \mathbb{R}^+_{3x3}$ to penalize the sum of change in state over all steps.

Sometimes an additional term $\bar{v}'\boldsymbol{\mathcal{R}}\bar{v}$ called the "input cost" is used to penalize the sum of change in input over all steps. When using voltage-source inverters, we can set $\boldsymbol{\mathcal{R}} = 0$ because changing the terminal voltage of is not associated with any significant drawbacks, so this term is not included.

The CFTOC problem can is defined as

$$J_0^*(\lambda(t)) = \min_{\mathcal{V}_{0\to N}} \; J_0(\lambda(0), \mathcal{V}_{0\to N}), \tag{19a}$$

$$\text{subj. to } \; \lambda_{k+1} = f(\lambda, \bar{v}), k = 0, \ldots, N-1, \tag{19b}$$

$$\lambda_k \in \Lambda, \bar{v}_k \in \mathcal{V}, k = 0, \ldots, N-1, \tag{19c}$$

$$\lambda_N \in \Lambda_f, \tag{19d}$$

$$\lambda_0 = \lambda(0), \tag{19e}$$

where J_0^* is the optimal cost or value function, Λ_f is the terminal region that the final flux λ_N must be in by the Nth step, and λ_0 is the defined starting state which is the same as the known state it is currently in $\lambda(0)$. A simple definition of the terminal region Λ_f is an area within some ϵ distance from the desired state λ^*,

$$\Lambda_f = \lambda^* + \epsilon, \epsilon \in \mathbb{R}^3. \tag{20}$$

There exists at least one optimum cost and trajectory if $\mathcal{V}_{0\to N}$ is compact and $f(\lambda, \bar{v})$ and $\bar{v}'\mathbf{Q}\bar{v}$ are continuous. The optimal output trajectory to the problem is denoted

$$\mathcal{V}^*_{0\to N} = \{\bar{v}^*_0, \bar{v}^*_1, \ldots, \bar{v}^*_{N-1}\}. \tag{21}$$

At $t = 0$ the first solution of the trajectory is the input to the system, at $t = 1$ the CFOTC problem is re-solved and first input of the new trajectory is the input to the system. This process is repeated indefinitely

$$\bar{v}(0) = \bar{v}^*_{0|0}(\lambda(0)), \tag{22a}$$

$$\bar{v}(1) = \bar{v}^*_{1|1}(\lambda(1)), \tag{22b}$$

$$\vdots \tag{22c}$$

$$\bar{v}(t) = \bar{v}^*_{t|t}(\lambda(t)). \tag{22d}$$

In each case, the horizon length is always N time steps ahead of the current time, thus the horizon is constantly being pushed further ahead in time, or "receding" from the present viewpoint.

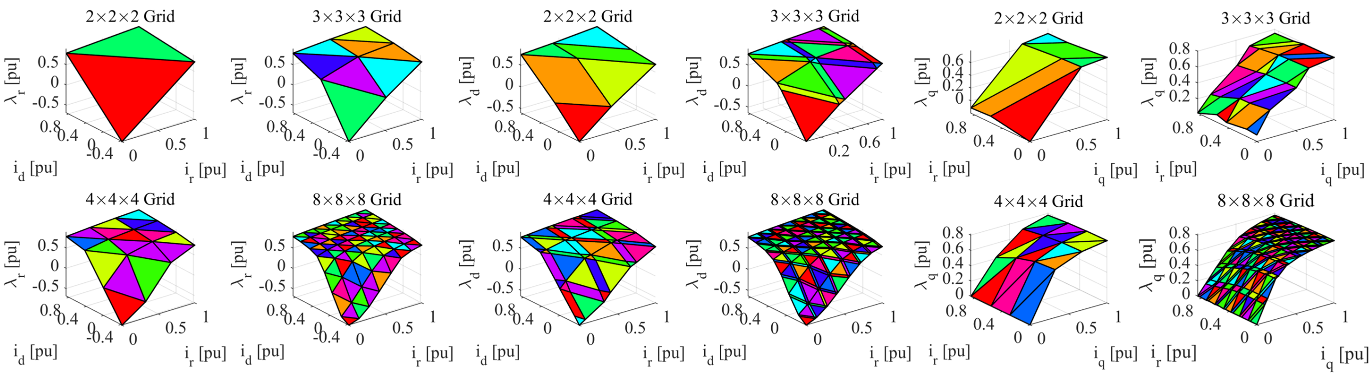

Fig. 4: PWA using $3 \times 3 \times 3$, $4 \times 4 \times 4$, $5 \times 5 \times 5$ and $8 \times 8 \times 8$ regularly sampled current grids: (left) λ_r vs i_d and i_d sliced at $i_q = 0$, (middle) λ_d vs i_r and i_d sliced at $i_q = 0$, (right) λ_q vs i_q and i_r sliced at $i_d = 0$.

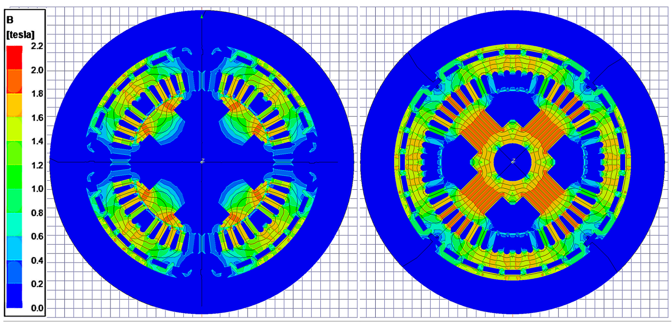

Fig. 5: WRSM cross section showing a saturated flux density B distribution in Tesla at $i_q = 1$[pu] (left), and $i_d = 1$[pu] (right)

TABLE II: WRSM Motor Drive Parameters

Parameter	**Value**
Turns ratio N_f/N_s	39
Pole pairs	2
Stator resistance	11.732 mΩ
Rotor resistance (stator referred)	5.461 mΩ
Shaft inertia	22.76E-3 kg m^2
Switching frequency	10 kHz
Sampling frequency	20 kHz
Nameplate r-axis inductance L_r	1.956 mH
Nameplate d-axis inductance L_d	2.420 mH
Nameplate q-axis inductance L_q	0.789 mH
DC-link voltage	325 V
Maximum power	65 kW
Maximum torque	220 Nm

TABLE III: MPC Simulation Parameters

State Space	**Cost**
$A = D = \begin{bmatrix} 0 & 0 & 0 \\ 0 & 0 & 0 \\ 0 & 0 & 0 \end{bmatrix}$	$P = \begin{bmatrix} 1 & 0 & 0 \\ 0 & 1 & 0 \\ 0 & 0 & 1 \end{bmatrix}$
$B = C = \begin{bmatrix} 1 & 0 & 0 \\ 0 & 1 & 0 \\ 0 & 0 & 1 \end{bmatrix}$	$Q = \begin{bmatrix} 1 & 0 & 0 \\ 0 & 1 & 0 \\ 0 & 0 & 1 \end{bmatrix}$

Let $c_t : \mathbb{R}^3 \to \mathbb{R}^3$ denote the RHC control law that associates an optimal input $\bar{v}^*_{t|t}$ after solving the CFTOC to the state $\lambda(t)$

$$c_t(\lambda(t)) = \bar{v}^*_{t|t}. \tag{23}$$

By combining the control law for any arbitrary positive time k (denoted c_k), with the system plant (equation 11) the closed-loop control equation c_{cl} is

$$c_{cl}(\lambda(k)) \triangleq \lambda(k+1) = T_s c_k(\lambda(k)), k \geq 0. \tag{24}$$

IV. Results

The CFTOC problem in equation 19 is solved using the Multi-Parametric Toolbox 3.0 (MPT3), which is uniquely designed to solve MPC with PWA system functions [23]. As shown in Figure 1, the measured state flux λ is calculated using the feedback current i and the PWA map in equation 13.

The MPT3 solver solves the CFTOC problem in equation 19 using a linear complementarity problem (LCP) solver that can solve linear problems (LP) and quadratic problems (QP) [24]. The output is a (completly seperate) PWA function which has a different function for each combination of active and inactive equality constraints.

A 65 kW WRSM with the parameters listed in Table II is used to validate the MPLPT formulation and solutions. Figure 5 shows a cross section of the machine.

The MPC controller is built using the MPT3 toolbox in a Matlab-Simulink simulation, and has the parameters shown in table III and a horizon length of $N = 2$.

The simulation of a torque and speed step using the described MPC controller is shown in Figure 6. The controller is programmed and simulated in $r\alpha\beta$ but for plotted and descrbied in rdq for simplicity. The simulation begins by fluxing up the rotor flux λ_r with a reference flux λ^*_r which by the cross-coupling mutual inductance also fluxes the stator d-axis flux λ_d. The rotor requires a constant flux reference to sustain its flux throughout the simulation. Then at $t = 0.2$ s a 2000 rpm speed step is initiated using a q-axis flux λ^*_q which is controlled by a PI speed controller. The speed step briefly takes the machine near its limit in torque (100 Nm/p or 200 Nm out of 220

Nm). Then after the transients have settled, at $t = 0.4$ s a 25 Nm/p torque step begins. The transient response of the MPC controller adequately shows the feasibility of MPC for the WRSM.

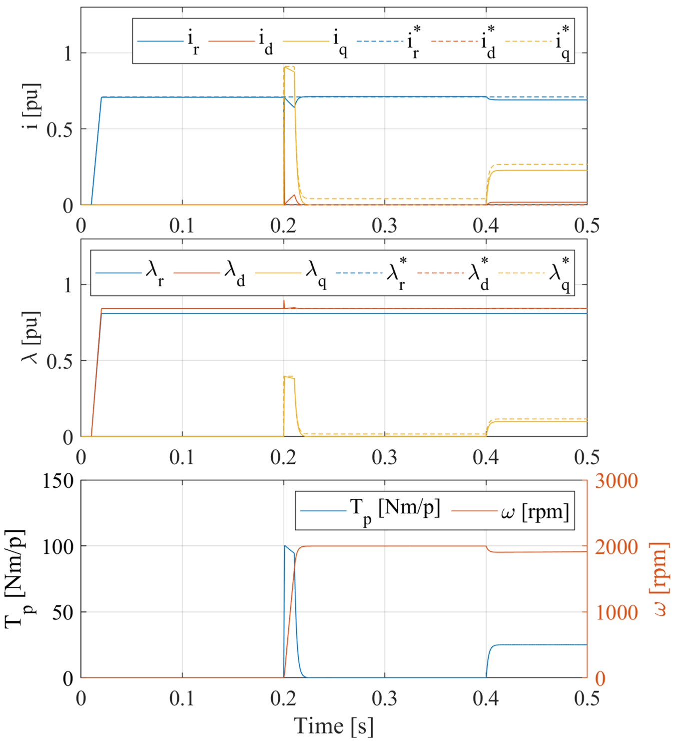

Fig. 6: Torque step, Speed step using MPC on a simulated WRSM

V. Conclusion

In this study the dynamic equations of the WRSM were redefined using a Piecewise-Affine (PWA) function to model the highly nonlinear flux-linkage relationship between current and flux in the machine. A model predictive controller (MPC) was formulated and implemented in a simulation environment, showing adequate results and proving that that the novel dynamic state space model in conjunction with MPC is viable for speed and torque control of the WRSM.

References

[1] A. Di Gioia, I. P. Brown, Y. Nie, R. Knippel, D. C. Ludois, J. Dai, S. Hagen, and C. Alteheld, “Design and Demonstration of a Wound Field Synchronous Machine for Electric Vehicle Traction With Brushless Capacitive Field Excitation,” *IEEE Trans. Ind. Appl.*, vol. 54, no. 2, pp. 1390–1403, Mar. 2018.

[2] N. Bedetti, S. Calligaro, and R. Petrella, “Stand-Still Self-Identification of Flux Characteristics for Synchronous Reluctance Machines Using Novel Saturation Approximating Function and Multiple Linear Regression,” *IEEE Trans. Ind. Appl.*, vol. 52, no. 4, pp. 3083–3092, Jul. 2016.

[3] H. Chen, C. Sun, and Q. Wang, “Analysis of Flux-Linkage Characteristics of Switched Reluctance Linear Generator,” *IEEE Trans. Appl. Supercond.*, vol. 24, no. 3, pp. 1–5, Jun. 2014.

[4] H. Chen, W. Yan, and Q. Wang, “Electromagnetic Analysis of Flux Characteristics of Double-Sided Switched Reluctance Linear Machine,” *IEEE Trans. Appl. Supercond.*, vol. 26, no. 4, pp. 1–7, Jun. 2016.

[5] P. Haghgooei, B. Nahid-Mobarakeh, N. Takorabet, and D. Arab-Khaburi, “Online Stator Flux Estimation for a Wound Rotor Synchronous Machine (WRSM),” in *Ind. Appl. Soc. IEEE-IAS Annu. Meet.*, pp. 1–6, Oct. 2020, iSSN: 2576-702X.

[6] P. Haghgooei, E. Jamshidpour, N. Takorabet, D. Arab-khaburi, and B. Nahid-Mobarakeh, “Magnetic Model Identification of Wound Rotor Synchronous Machine Using a Novel Flux Estimator,” *IEEE Trans. on Ind. Applicat.*, pp. 1–1, 2021.

[7] K. Liu, J. Feng, S. Guo, L. Xiao, and Z.-Q. Zhu, “Identification of Flux Linkage Map of Permanent Magnet Synchronous Machines Under Uncertain Circuit Resistance and Inverter Nonlinearity,” *IEEE Trans. Industr. Inform.*, vol. 14, no. 2, pp. 556–568, Feb. 2018.

[8] Y. Nie, D. C. Ludois, and I. P. Brown, “Deadbeat-Direct Torque and Flux Control of Wound Field Synchronous Machine at Low Sampling to Fundamental Frequency Ratios,” *IEEE Trans. Ind. Appl.*, vol. 55, no. 4, pp. 3813–3822, Jul. 2019.

[9] M. Seilmeier and B. Piepenbreier, “Identification of steady-state inductances of PMSM using polynomial representations of the flux surfaces,” in *IECON - 39th Annu. Conf. IEEE Ind. Electron. Soc.*, pp. 2899–2904, Nov. 2013, iSSN: 1553-572X.

[10] E. Armando, R. I. Bojoi, P. Guglielmi, G. Pellegrino, and M. Pastorelli, “Experimental Identification of the Magnetic Model of Synchronous Machines,” *IEEE Trans. Ind. Appl.*, vol. 49, no. 5, pp. 2116–2125, Sep. 2013.

[11] E. Armando, P. Guglielmi, G. Pellegrino, and R. Bojoi, “Flux linkage maps identification of synchronous AC motors under controlled thermal conditions,” in *2017 IEEE Int. Electr. Mach. Drives Conf. (IEMDC)*, pp. 1–8, May. 2017.

[12] Q. Wang, G. Zhang, G. Wang, C. Li, and D. Xu, “Offline Parameter Self-Learning Method for General-Purpose PMSM Drives With Estimation Error Compensation,” *IEEE Trans. Power Electron.*, vol. 34, no. 11, pp. 11 103–11 115, Nov. 2019.

[13] A. Doria-Cerezo, V. I. Utkin, R. S. Munoz-Aguilar, and E. Fossas, “Control of a Stand-Alone Wound Rotor Synchronous Generator: Two Sliding Mode Approaches via Regulation of the d-Voltage Component,” *IEEE Trans. Control Syst. Technol.*, vol. 20, no. 3, pp. 779–786, May. 2012.

[14] D. Uzel, V. Smidl, and Z. Peroutka, “Gradient descent maximum torque control up to the base speed of wound rotor synchronous motors,” in *2017 IEEE Int. Conf. Mechatron.*, pp. 1–6, Dec. 2016.

[15] A. Dòria-Cerezo, C. Batlle, and G. Espinosa-Pérez, “Passivity-based control of a wound-rotor synchronous motor,” *IET Control Theory & Appl.*, vol. 4, pp. 2049–2057, 2010.

[16] N. Yang, B. Nahid-Mobarakeh, A. Corne, and J.-P. Martin, “Multiple-vector-based predictive direct current control for a wound rotor synchronous machine drive,” in *Ind. Appl. Soc. IEEE-IAS Annu. Meet.*, pp. 1–9, Oct. 2016.

[17] Y. Kim and K. Nam, “Copper-Loss-Minimizing Field Current Control Scheme for Wound Synchronous Machines,” *IEEE Trans. Power Electron*, vol. 32, no. 2, pp. 1335–1345, Feb. 2017.

[18] I. Canay, “Causes of discrepancies on calculation of rotor quantities and exact equivalent diagrams of the synchronous machine,” vol. PAS-88, pp. 1114–1120.

[19] M. Preindl and S. Bolognani, “Optimal state reference computation with constrained mtpa criterion for pm motor drives,” *IEEE Trans. Power Electron.*, vol. 30, no. 8, pp. 4524–4535, 2015.

[20] M. Preindl, “Robust control invariant sets and lyapunov-based mpc for ipm synchronous motor drives,” *IEEE Trans. Ind. Electr.*, vol. 63, no. 6, pp. 3925–3933, 2016.

[21] P. Samuel and S. Levy, *Projective Geometry*, ser. Undergraduate Texts in Mathematics. Springer New York, 1988.

[22] F. Borrelli, A. Bemporad, and M. Morari, “Predictive control for linear and hybrid systems,” 2017.

[23] M. Herceg, M. Kvasnica, C. N. Jones, and M. Morari, “Multi-parametric toolbox 3.0,” in *2013 European Control Conference (ECC)*, pp. 502–510, 2013.

[24] C. N. Jones and M. Morrari, “Multiparametric linear complementarity problems,” in *Proceedings of the 45th IEEE Conf. on Decision and Control*, pp. 5687–5692, 2006.